JOURNAL OF MATERIALS SCIENCE 25 (1990) 2056–2062

Metal and semi-metal precipitates in Nuclepore membranes

DAHN KATZEN, SHIMON REICH*
Department of Materials Research, Weizmann Institute of Science, Rehovot, Israel 76100
STEPHEN MAZUR
The Central Research and Development, E.I. du Pont de Nemours and Company, Experimental Station, Wilmington, Delaware 19898, USA

Au, Pt, Ag, Sb, Te, In and Ge were precipitated by a salt-reducing agent reaction into the pores of Nuclepore membranes 10 to 600 nm pore size range. The precipitates form filament-like structures inside the pores and a dendritic growth on the surface. The permeation of water as a function of pore size in the Nuclepore membranes was measured by tracing the diffusion through the membrane with tritium. The results are modelled and theoretical predictions are compared with the experimentally observed kinetics for metal deposition in the membranes. Also the d.c. electrical properties of the metal precipitates were measured. The anisotropic electrical properties of these systems are dictated by the morphology of the precipitated metal on the membrane.

1. Introduction

Electrochemical or chemical reactions coupled to an ion transport process through a polymer membrane may lead to precipitation of metallic and non-metallic interlayers, or to a set of periodic interlayers parallel to the membrane surface. Examples of the above are: sharply defined layers of $BaSO_4$ in agar [1]; precipitate membranes [2]; electrochemical deposition of metals in an electroactive polymer [3, 4]; electroless deposition of silver as an interlayer within polymer films [5, 6].

In this work the formation of microfilament structures of metallic and semi-metallic nature inside Nuclepore (NP) membranes and perpendicular to the membrane surface is presented. These microfilament structures are created by counter-current diffusion of a salt and a reducing agent from opposite sides of a NP membrane. These hydrophilic polyvinyl-pyrrolidone (PVP) coated polycarbonate membranes have straight-through pores created by a two step process of irradiation and etching, distributed randomly and penetrating the surface at an angle of incidence of $\pm 34°$ [7, 8]. Upon the encounter of the two diffusional fronts, the salt from one side, and the reducing agent from the other side, inside the pores of the NP membrane a precipitation of a metal or semi-metal, or a semi-conductor is achieved in the form of thin filaments filling the pores. The diameter of the filaments is controlled by the pore size, characteristically in the range of 10 to 600 nm. The uniformity of the filament diameters is dictated by the uniformity of the NP pores which is better than 20%. In this work we present the formation of micro-filaments of gold, platinum, silver, nickel, antimony, and indium metals, a semi-metal tellurium and a semi-conductor germanium. We have studied the permeation of platinum through the NP membranes as a function of pore size. We followed precipitation kinetics of some of the metals and the morphology of the deposited filaments. We investigated the electrical d.c. conductivity of these metal polymer composites parallel and perpendicular to the membrane surface as a function of pore size.

2. Experimental procedure

NP membranes were purchased from Nuclepore Corporation in the size range of 10 to 600 nm pore size. These membranes were equilibrated in triple distilled water for a few hours before the precipitation experiments began. All solutions were prepared using triple distilled water and using analytical grade reagents. The conditions for the precipitation of metals and semi-metals in NP membranes are summarized in Table I. The NP membranes were mounted into a diffusion PMMA cell, stirred on both sides with magnetic stirrers, see Fig. 1, the volume of the solutions on both sides of the membrane was 17 ml and the surface exposed to solutions was 5 cm^2. The experiment was begun by simultaneously adding 17 ml of the salt solution on one side of the membrane and a reducing agent on the other. After countercurrent exposure for a desired time, both halves of the cell were quickly emptied and washed with excess water. All experiments were performed at 25° C. Surface d.c. conductivity of the membrane metal composite was measured between the centre and the ring of a bull's-

*Author to whom all correspondence should be addressed.

0022–2461/90 $03.00 + .12

TABLE I

Metal	Salt	Salt concentration (10^{-3} M)	Solvent	Reducer concentration (10^{-3} M)	Solvent	Time of reaction (min)	NP pore size (nm)
Au	$NaAuCl_4 \cdot 2H_2O$	10	H_2O	$[NaBH_4] = 20$	H_2O	2 – 120	10, 50, 100, 400
Pt	$H_2PtCl_6 \cdot 6H_2O$	5	H_2O	$[NaBH_4] = 2$	H_2O	2 – 45	10, 50, 100, 400
Ag	$AgBF_4$	1	H_2O	$[NaBH_4] = 10$	H_2O	18	50
Ni	$NiCl_2 \cdot H_2O$ + $Ni(CH_3CO_2)_2 \cdot 4H_2O$ + 10% NH_4OH	50 20	H_2O	$[KBH_4] = 10$	10% Ethanol 1% NH_4OH	2 × 10	100
Sb	K(SbO) Tartarate 1/2 H_2O	23	H_2O	$[KBH_4] = 210$	10% Ethanol 3% NH_4OH	~5	100
In	$InCl_3$ Tartaric acid	80 204	H_2O	$[KBH_4] = 5.2$	5% Ethanol 0.15% NH_4OH	15	100
Te	$TeCl_4$	88	Ethylene Glycol	$[KBH_4] = 60$	Ethylene Glycol + 1% KOH 5M	5 – 125	100
Te	$TeCl_4$	80	Ethanol Absolute	$[NaBH_4] = 56$	80% Ethanol 20% H_2O	5 – 125	100
Te	$TeCl_4$	80	Ethanol Absolute	$[NaBH_4] = 100$	70% Ethanol 30% H_2O	5 – 125	10
Ge	$GeCl_4$	100	Ethanol Absolute	$[KBH_4] = 60$	Ethylene Glycol + 1% KOH 5M	24	10

eye gold pattern spattered on the membrane's surface using indium pressure contacts. Conductivity perpendicular to the surface, through the membrane, was measured between two 1 cm^2 indium disks pressed against the membrane.

3. Results

The morphology of gold, platinum and tellurium inside 100 nm pores was studied by transmission electron microscopy (TEM) and by scanning electron microscopy (SEM). A TEM micrograph taken for a gold deposit shows that at the beginning of the precipitation process small crystallites of gold grow on the pore walls, see Fig. 2; subsequently the pores are filled as shown in Fig. 2 for a tellurium deposit. As the pores are filled a dendritic growth appears on both sides of the membrane; on the dull side of the membrane, which faces the salt solution during the deposition process, the dendrites are feather like, and needle like dendritic growth is observed on the smooth shining side. These morphologies are shown in SEM micrographs in Fig. 3. X-ray diffraction was used to verify pure metallic gold, platinum and tellurium in the precipitate. The measured tellurium lines are tabulated against PDF values in Table II.

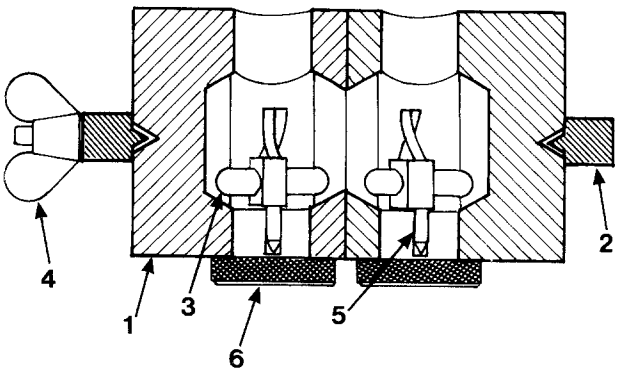

Figure 1 Diffusion cell set up: 1 transparent cell; 2, 4 clamp assembly; 3 stirring propeller and magnet; 5, 6 shaft for stirrer.

The kinetics of deposition for gold and platinum in a 10 nm pore size membrane from an aqueous solution are shown in Figs 4 and 5. Tellurium precipitation kinetics from ethylene glycol in a 100 nm pore size membrane are shown in Fig. 6. An almost linear uptake of metal is observed in the first 10 to 20 min time period followed by a saturation phenomenon.

The d.c. surface resistivity, as measured on the dull side of the membrane, was measured as a function of metal loading in 100 nm pore size membranes. We observe high anisotropy of resistivity for the lowest loading value of ~0.1 mg cm^{-2} (Fig. 7). The transverse resistivity is ~17 Ω cm^{-2} (Fig. 8) and the membrane thickness is 6 × 10^{-4} cm. Isotropic behaviour should yield a value of ~3 × 10^4 Ω per unit area for the surface resistivity, we observe however ~10^8 Ω per

TABLE II

d_{PDF} (nm)	I/I_1	$d_{measured}$ (nm)	Strength
0.3230	100	0.321	S
0.2351	37	0.234	M
0.2228	31	0.223	MW
0.1980	8	0.196	W
0.1835	20	0.183	W
0.1781	7	0.176	VW
0.1616	12	0.161	W
0.1479	13	0.146	W
0.1383	7	0.137	VW
		0.117	VW
0.2087	11	0.205	VW
0.3860	20	0.386	W

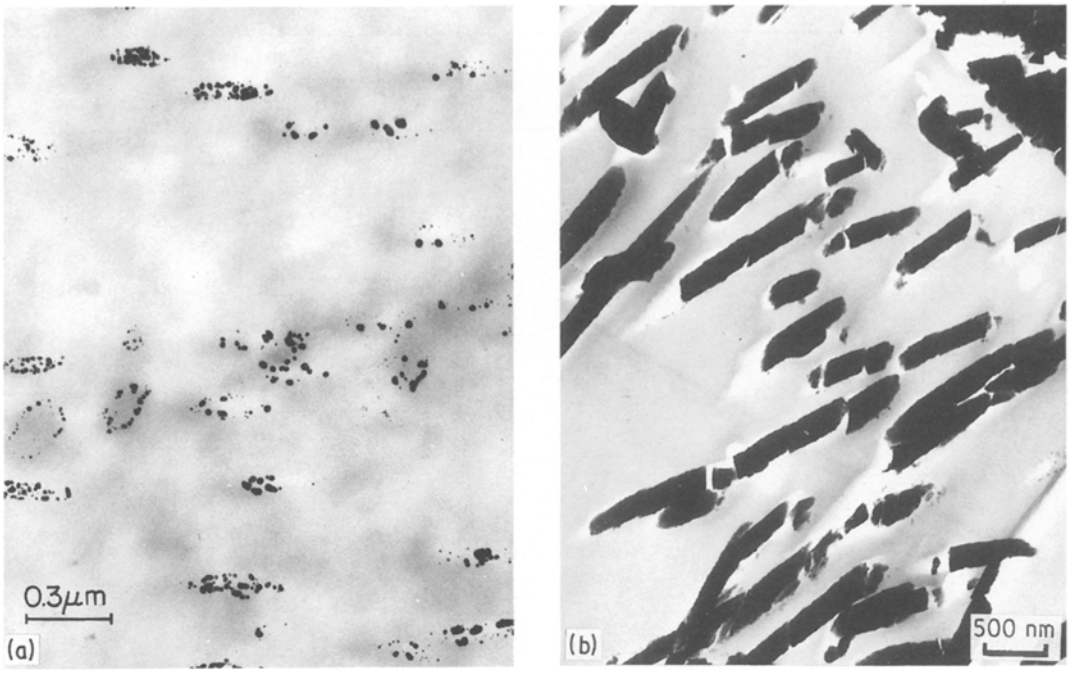

Figure 2 (a) Early stages for the deposition of gold in a 100 nm pore size NP membrane. (b) Late stage for deposition of tellurium in a 100 nm pore size NP membrane.

square. This anisotropy disappears for higher loadings of the tellurium metal.

4. Discussion

To estimate the deposition rates of various metals in NP membranes from aqueous solutions it is enough to know the value of the permeability of water per unit pore area, the number of pores per unit area of membrane, as well as its thickness. This is true only when the diffusion step of the salt and the reducer in the pore is slow in comparison to the kinetics of the reduction process. Also it is assumed that the diffusion of various ions under study is of the same order of magnitude as that observed in water. To characterize the diffusion of water through the NP membranes we used tritiated water on one side of the membrane (2×10^{-2} mq ml^{-1}) and regular water on the other. 100 μl samples were taken at 1 min intervals to measure the permeability. In the following discussion the tritiated water is referred to as solute.

Consider the following set-up. Two cells separated by a Nuclepore membrane of width l, and average pore density N pores per unit area. Each pore being of radius r. In one cell we put solvent with a solute of concentration C_0, and in the other cell pure solvent. The liquid in each cell stirred by a magnetic stirrer rotating at angular velocity ω. Hydrodynamic theory tells us that near the walls of the cell, and this includes

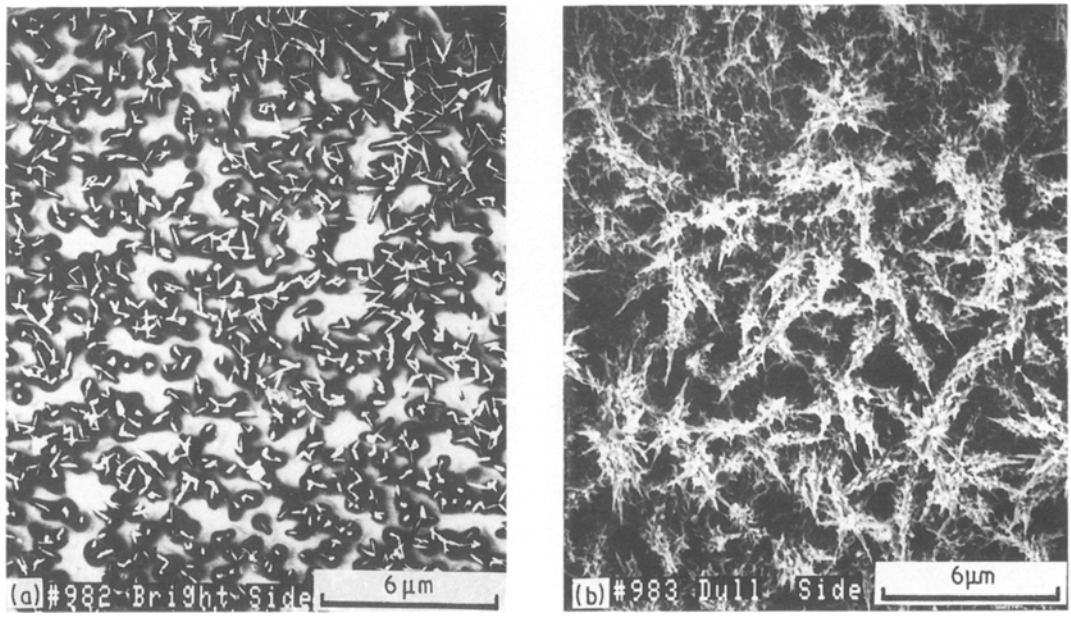

Figure 3 Dendrite growth of tellurium in a late stage of deposition. (a) Bright shiny side of the membrane facing the reducing agent. (b) Dull side of the membrane facing the tellurium salt during the precipitation process.

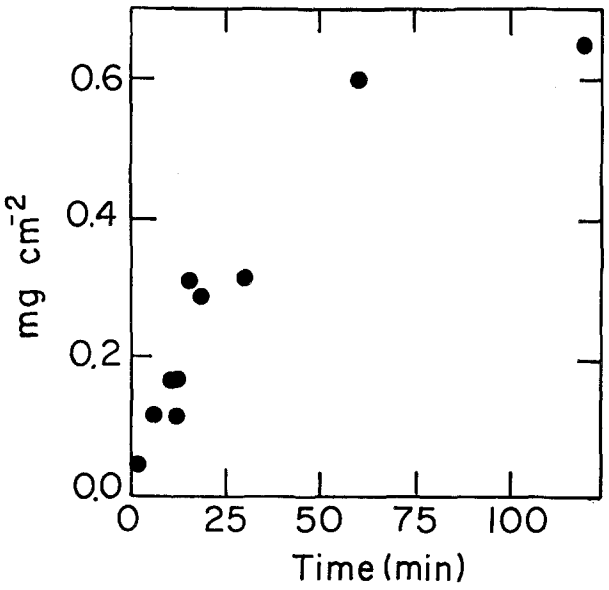

Figure 4 Deposition kinetics of gold in a 10 nm pore size NP membrane. $NaAuCl_4 \cdot 2H_2O$–0.01 M in water – $NaBH_4$–0.02 M in water.

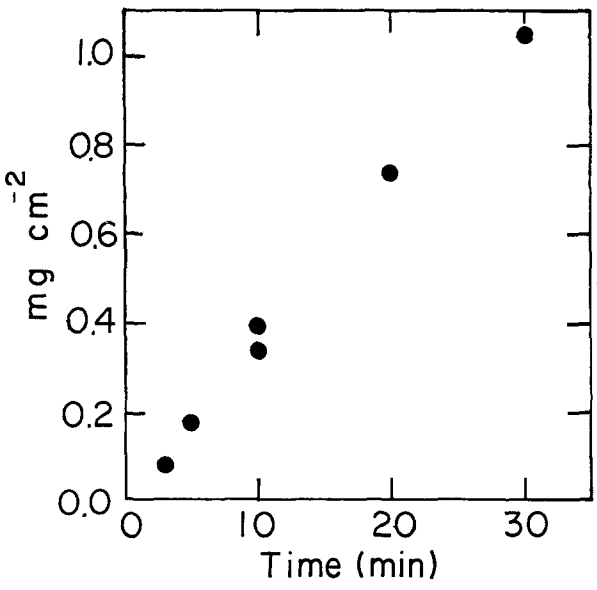

Figure 6 Deposition kinetics of tellurium in a 100 nm pore size NP membrane. $TeCl_4$–0.08 M in Ethyleneglycol – KBH_4–0.06 M Ethyleneglycol + 0.5 ml KOH 5M in 50 ml solution.

the membrane, there is a layer in which the flow is laminar of width $W \sim (\nu/\omega)^{1/2}$, where ν is the kinematic viscosity of the solvent. In this layer we don't have turbulent mixing, and we assume that mass transport across flow lines occurs via diffusion alone. There exists a concentration gradient in an area around the membrane. The average thickness of this region, L, is smaller than W since the kinematic viscosity is much greater than the diffusion coefficient, in the system under study (water) [10].

We are interested in the permeability of the membrane to the solute. To obtain an expression for the permeability we note that the amount of solute diffusing through the membrane is proportional to the area of the membrane, A, the concentration difference between the cells, ΔC, the amount of time allowed, t, and inversely proportional to the width of the membrane, l.

$$\Delta Q \propto \frac{A\Delta Ct}{l} \tag{1}$$

The proportionality constant is the permeability P. Under equilibrium conditions the value obtained for P (for these membranes) would be $D \times N\pi r^2$ the diffusion coefficient of the solute in the solvent, multiplied by the effective open area. However, in our set up we don't have equilibrium, we have a steady state, and under these circumstances P is slightly more complicated.

The region of interest is the unstirred boundary layer on both sides of the membrane, and the membrane itself. In Fig. 9 we label the region to the left of the membrane, a, the membrane, b, and the region to the right, c. The concentration of solute outside of the unstirred layers is kept uniform by stirring, so the

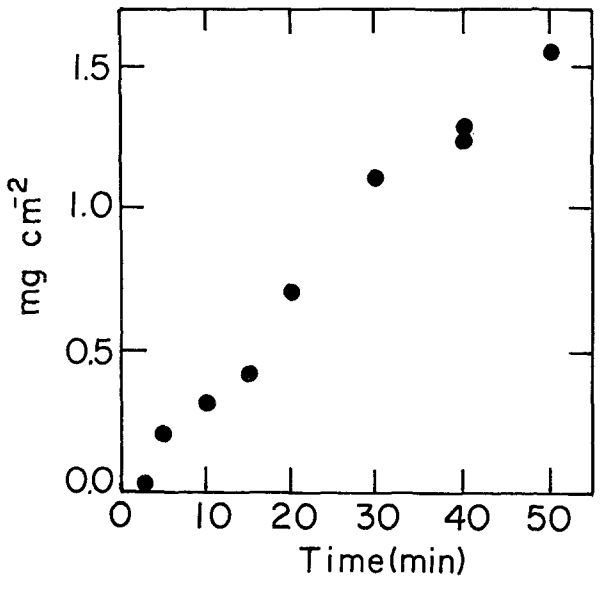

Figure 5 Deposition kinetics of platinum in a 10 nm pore size NP membrane. $H_2PtCl_6 \cdot 6H_2O$–0.005 M in water – $NaBH_4$–0.02 M in water.

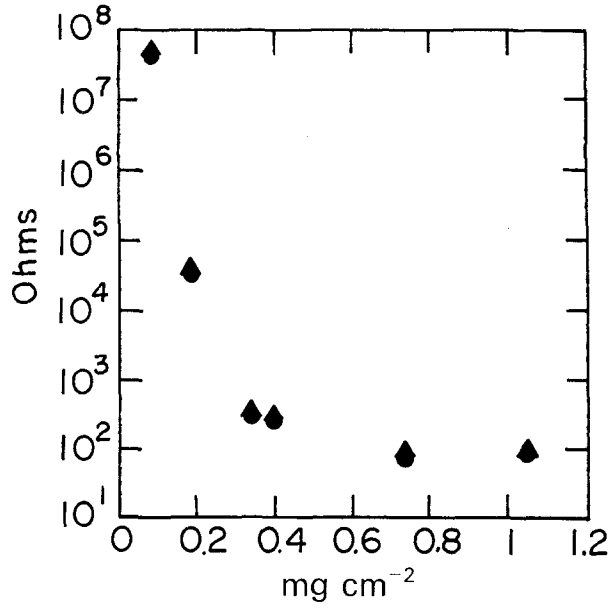

Figure 7 Surface resistivity of tellurium deposit in 100 nm pore size NP membrane as a function of metal loading.

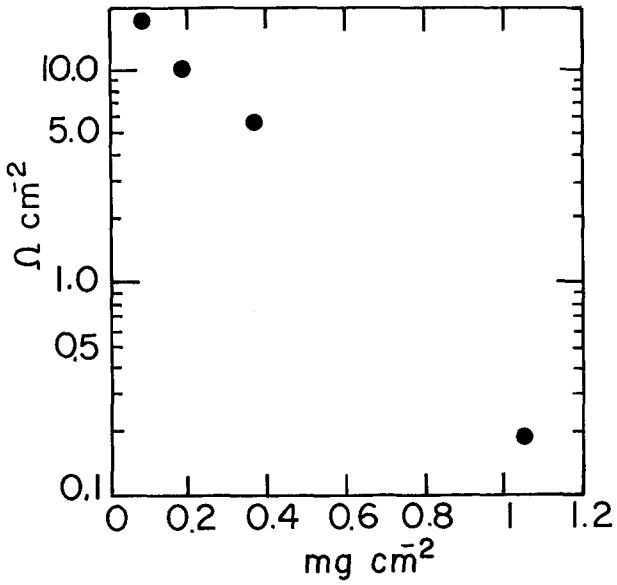

Figure 8 Transverse resistivity of tellurium deposit in 100 nm pore size NP membrane as a function of metal loading.

concentration gradient in this region is zero. We assume that the amount of solute which diffuses through a, b and c is large enough to be measured, but too small to change the concentrations in the stirred regions. In addition we assume a steady state situation, therefore the amount of solute per unit time, $\Delta Q/t$, diffusing through each of the three regions a, b, c must be equal, i.e.

$$\frac{\Delta Q_a}{t} = \frac{\Delta Q_b}{t} = \frac{\Delta Q_c}{t} \tag{2}$$

Now the amount of solute per unit time per unit area is the flux density, therefore $\Delta Q/t = JA$, where A is the area across which the diffusion is taking place, and J is the flux density. Using these facts Equation (2) becomes

$$J_a A_a = J_b A_b = J_c A_c \tag{3}$$

Using Fick's Law, $J = D\Delta C/x$, where D is the diffusion coefficient and $\Delta C/x$ is the concentration gradient over distance x, and using the fact that $A_a = A_c$ and $A_b = N\pi r^2 A_a$ (the open area in the membrane) in Equation (3) yields

$$D\frac{C_0 - C_1}{L} = DN\pi r^2 \frac{C_1 - C_2}{l} = D\frac{C_2 - C_3}{L} \tag{4}$$

where L is the width of the unstirred boundary layer, l is the membrane width, N is the pore density, r is the pore radius, C_0 is the concentration in the right cell, C_1 is the concentration on the right edge of the membrane, C_2 is the concentration on the left edge of the membrane and C_3 is the concentration in the left cell.

From this equation we obtain

$$C_0 - C_1 = C_1 - C_2 \tag{5}$$

and

$$\frac{C_0 - C_1}{L} = N\pi r^2 \frac{C_1 - C_2}{l} \tag{6}$$

$$N\pi r^2 \frac{C_1 - C_2}{l} = \frac{C_2 - C_3}{L} \tag{7}$$

Solving Equation (5) for C_2 and using this result in Equation (6) and solving for C_1, we find

$$C_1 = \left[\left(\frac{1}{L} + \frac{N\pi r^2}{l}\right) C_0 + \frac{N\pi r^2}{l} C_3\right] \Big/ \left(\frac{1}{L} + 2\frac{N\pi r^2}{l}\right) \tag{8}$$

Similarly, solving Equation (5) for C_1 and using this result in Equation (7) and solving for C_2, we get

$$C_2 = \left[\frac{N\pi r^2}{l} C_0 + \left(\frac{1}{L} + \frac{N\pi r^2}{l}\right) C_3\right] \Big/ \left(\frac{1}{L} + 2\frac{N\pi r^2}{l}\right) \tag{9}$$

Therefore

$$C_1 - C_2 = \frac{C_0 - C_3}{2LN\pi r^2\left(\frac{1}{l}\right) + 1} \tag{10}$$

which we choose to express as

$$C_1 - C_2 = \frac{C_0 - C_3}{L\left[\left(\frac{2\pi N}{l}\right)^{1/2} r\right]^2 + 1} \tag{11}$$

Now, applying Fick's law to the membrane, and using Equation (11), we find

$$J_b = D\frac{C_1 - C_2}{l} = \frac{D/l}{L\left[\left(\frac{2\pi N}{l}\right)^{1/2} r\right]^2 + 1}(C_0 - C_3) \tag{12}$$

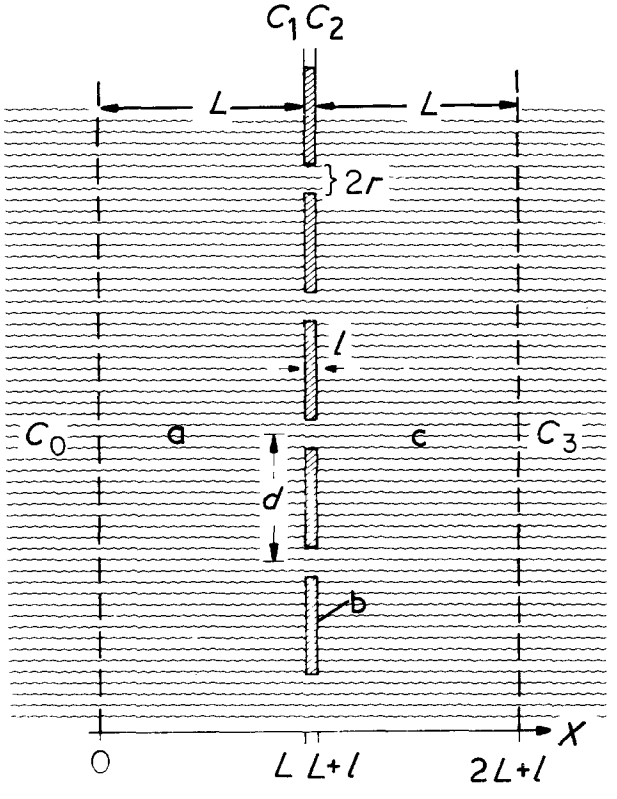

Figure 9 Schematic representation of the diffusion layers on both sides of the Nuclepore membrane.

and

$$\frac{\Delta Q}{t} = J_b A_b = \frac{DN\pi r^2}{L\left[\left(\frac{2\pi N}{l}\right)^{1/2} r\right]^2 + 1} \times \frac{C_0 - C_3}{l} \tag{13}$$

Comparing Equation (13) with Equation (1), we see that the permeability of the membrane is given by

$$P = \frac{DN\pi r^2}{L\left[\left(\frac{2\pi N}{l}\right)^{1/2} r\right]^2 + 1} \tag{14}$$

and per unit pore area

$$P_0 = \frac{P}{N\pi r^2} = \frac{D}{L\left[\left(\frac{2\pi N}{l}\right)^{1/2} r\right]^2 + 1} \tag{15}$$

We can express P_0 entirely in terms of geometrical parameters of the system, by noting that if there are N pores per unit area, and $N = 1/d^2$, then d is the distance between pores. Then Equation (15) would become

$$P_0 = \frac{D}{L\left[\left(\frac{2\pi}{l}\right)^{1/2}\left(\frac{r}{d}\right)\right]^2 + 1} \tag{16}$$

In view of our theory, we do a least squares fit of the data to the equation

$$P_0 = \frac{D}{Lx^2 + 1} \tag{17}$$

where $x = (2\pi/l)^{1/2}(r/d)$ is a variable which uniquely defines a membrane, P_0 is the measured value of the permeability per unit pore area, and D and L are parameters to be determined by the minimization process. Therefore, we want to minimize

$$\sum_{i=1}^{n}\left(P_{0i} - \frac{D}{Lx_i^2 + 1}\right)^2 \tag{18}$$

Differentiating Equation (18) by D and setting equal to zero, yields

$$D = \sum_{i=1}^{n}\frac{P_{0i}}{\beta x_i^2 + 1}\Big/\sum_{i=1}^{n}\frac{1}{(\beta x_i^2 + 1)^2} \tag{19}$$

Similarly, differentiating Equation (18) by L and setting equal to zero, gives

$$D = \sum_{i=1}^{n}\frac{P_{0i}x_i^2}{(\beta x_i^2 + 1)^2}\Big/\sum_{i=1}^{n}\frac{x_i^2}{(\beta x_i^2 + 1)^3} \tag{20}$$

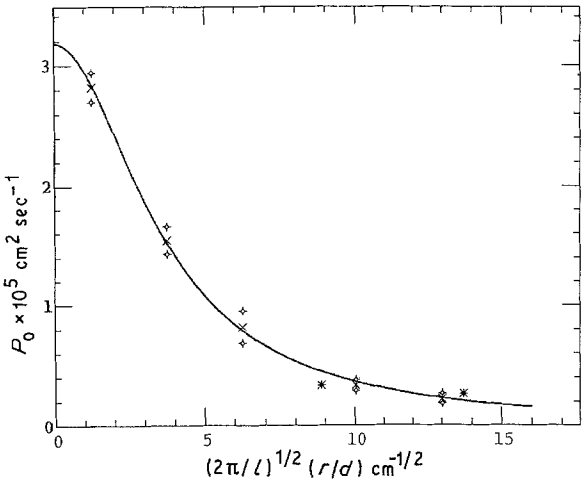

Figure 10 Permeability per unit pore area for water as a function of membrane "geometry". × – average value; -⊹- – measured values.

The value for D obtained from Equations (19) and (20) should be equal; this gives an implicit equation for L which is then solved numerically. The value of L is then used in either Equation (19) or Equation (20) to obtain D.

We observe that the above analysis fits the experimental data well, see Fig. 10; the continuous line represents the best fit, with $D_{[H_2O]} = 3.17 \times 10^{-5}$ cm^2 sec^{-1} and $L = 0.07$ cm as parameters. The value for D is comparable to that quoted in the literature [9]. We observe that the permeability per unit pore area decreases as the pore size increases – a result which is not intuitively trivial. The data for a series of pore sizes in the range 10 to 600 nm is tabulated in Table III.

We can now estimate the amount, Q, of platinum for example, deposited *inside* the pores of a 10 nm pore size membrane after 5 min, and compare with the experimental data in Fig. 5.

$$Q = \frac{P_0 t}{l} \times \frac{MW_{Pt}}{MW_{salt}} C_s A_p \tag{21}$$

where C_s is the concentration of the platinum salt, and A_p is the total pore area per unit area of membrane.

TABLE III Permeabilities of tritiated water

Pore diameter (μm)	Area of pore ($\times 10^{13}$ cm^2)	N pores (per cm^2)	Tota pore area ($\times 10^4$ cm^2)	Permeability/ membrane area cm^2 sec^{-1} $\times 10^8$	Permeability per pore cm^2 sec^{-1} $\times 10^{17}$	Permeability per unit pore area cm^2 sec^{-1} $\times 10^5$
0.01	7.8	6×10^8	4.2	1.4	2.3	2.9
0.01	7.8	6×10^8	4.2	1.3	2.1	2.7
0.03	70.7	6×10^8	42.4	6.1	10.1	1.4
0.03	70.7	6×10^8	42.4	7.0	11.7	1.7
0.05	196.3	6×10^8	117.8	8.0	13.4	0.7
0.05	196.3	6×10^8	117.8	11.2	18.7	0.95
0.08	502.7	6×10^8	301.6	8.6	14.4	0.3
0.08	502.7	6×10^8	301.6	11.4	18.9	0.4
0.1	785.4	3×10^8	235.6	7.8	26.0	0.3
0.2	3141.6	3×10^8	942.5	24.6	82.0	0.3
0.6	28274.3	3×10^7	848.2	15.1	503.4	0.2
0.6	28274.3	3×10^7	848.2	22.3	743.5	0.3

Substituting into Equation (21) the proper values from Table III for a 10 nm pore size membrane we get a platinum loading of 6×10^{-6} gr cm^{-2} as compared to 2×10^{-4} gr cm^{-2} observed experimentally. A direct measurement for the platinum salt in a conductometric experiment yields for P a value of 6.7×10^{-5} cm^2 sec^{-1} which gives a loading of 1.4×10^{-5} gr cm^{-2}. This discrepancy is apparently due to the dendritic morphology of the metal deposit. As shown by the TEM results (Fig. 2b), within the pores the precipitate forms needles whose major axes are oriented parallel to the pore. Because these materials are conductors, it is only necessary for the reagents to diffuse to opposite ends of each needle for reaction to occur. Once the length of the needles have grown to a significant fraction of l, this heterogeneous growth mechanism can proceed faster than the initial homogeneous reaction. This suggests that the electrical properties are strongly influenced by the anisotropy of crystalline growth and might be altered by the use of nucleating agents or other conditions which influence heterogeneous kinetics. SEM micrographs show that most of the metal is deposited in the dendritic form on the surface of the membrane. This phenomenon also explains the high anisotropy in d.c. conductivity observed in the early stages of deposition. At those stages indeed most of the precipitate is formed *inside* the membrane and thus a morphology of metallic mostly independent filaments is observed. Thus the specific conductivity through the membrane is $\sim 10^3$ times larger than the surface conductivity. When the dendritic growth is developed the filaments are connected through the dendrites and isotropic conductivity is observed.

Acknowledgements

We would like to thank Joseph Cohen and Geula Talmi from the Weizmann Institute and Conroy Osier from CR & D Du Pont for valuable assistance. In addition we would like to thank Prof. Joseph Jagur-Grodzinski for helpful discussions.

REFERENCES

1. E. P. HONIG, J. H. HENGST and P. HIRSCH-AYALON, *Ber. Bunsenges. Phys. Chem.* **72** (1968) 1231.
2. A. J. AYALON, *Membr. Sci.* **20** (1984) 43.
3. S. MAZUR and S. REICH, *J. Phys. Chem.* **90** (1986) 1365.
4. S. MAZUR and S. REICH, in Proceedings of the Conference on Integration of Polymer Science and Technology, Rolduc, Holland, April 1985 (Elsevier, Amsterdam, 1985) p. 265.
5. L. E. MANRING, *Polymer Communications* **28** (1987) 68.
6. L. E. MANRING and S. MAZUR, *J. Phys. Chem.* **90** (1986) 3269.
7. Nuclepore Specifications (Nuclepore Corporation Catalog, 1984).
8. R. E. KESTINE, "Polymer Membranes" (Wiley, New York, 1985) p. 305.
9. N. LAKSHMINARAYANAIAH, "Transport Phenomena in Membranes" (Academic Press, London, 1969) p. 320.
10. V. G. LEVICH, "Physicochemical Hydrodynamics" (Prentice Hall, Englewood Cliffs, N.J. 1962) Chap. 3.

Received 1 December 1988
and accepted 2 May 1989